Energy Conversion and Management 65 (2013) 41–49

Contents lists available at SciVerse ScienceDirect

Energy Conversion and Management

journal homepage: www.elsevier.com/locate/enconman

Particle swarm optimization based fuzzy logic controller for autonomous green power energy system with hydrogen storage

S. Safari, M.M. Ardehali *, M.J. Sirizi

Energy Research Center, Department of Electrical Engineering, Amirkabir University of Technology (Tehran Polytechnic), 424 Hafez Ave., Tehran 15825-4413, Iran

ARTICLE INFO

Article history:
Received 12 June 2012
Received in revised form 13 August 2012
Accepted 21 August 2012
Available online 11 October 2012

Keywords:
Fuzzy logic controller
Hybrid green power system
Optimization
Operation and maintenance costs
Loss of power supply probability

ABSTRACT

The objective of this study is to develop an optimized fuzzy logic controller (FLC) for operating an autonomous hybrid green power system (HGPS) based on the particle swarm optimization (PSO) algorithm. An electrolyzer produces hydrogen from surplus energy generated by the wind turbine and photovoltaic array of HGPS for later use by a fuel cell. The PSO algorithm is used to optimize membership functions of the FLC. The FLC inputs are (a) net power flow and (b) batteries state of charge (SOC) and FLC output determines the time for hydrogen production or consumption. Actual data for weekly residential load, wind speed, ambient temperature, and solar irradiation are used for performance simulation and analysis of the HGPS examined. The weekly operation and maintenance (O&M) costs and the loss of power supply probability (LPSP) are considered in the optimization procedure. It is determined that FLC optimization results in (a) reduced fluctuations in batteries SOC which translates into longer life for batteries and the average SOC is increased by 6.18% and (b) less working hours for fuel cell, when the load is met by wind and PV. It is found that the optimized FLC results in lower O&M costs and LPSP by 57% and 33%, respectively, as compared to its un-optimized counterpart. In addition, a reduction of 18% in investment cost is achievable by optimal sizing and reducing the capacity of HGPS equipment.

1. Introduction

Solar and wind energy are inexpensive, environmental friendly, non-depletable, and could serve as potential sources of alternative energy [1–3]. A green power system (GPS) that benefits from solar and wind energy often encounters noticeable limitations that originate from the intermittent nature of its contributing source [4]. To overcome the intermittency problem in power generation and increase reliability to meet continuous loads, two or more systems are used I hybrid from in conjunction with storage devices [5]. While batteries have been used to reduce or compensate for the intermittency caused by adverse effects of time varying weather conditions, they have low useful life and hydrogen-based fuel cells are also integrated into hybrid GPS (HGPS) as viable solutions [6,7].

To regulate the energy flow among the different components of a HGPS, a control system is necessary. Numerous studies have been performed on control of HGPS with hydrogen storage. In a study, a neural network control system is programmed to learn over time to use system resources more efficiently by adjusting the energy storage strategy to variations in power production and demand [8], but it needs historical data to be efficient. In another study, an un-optimized fuzzy logic controller (FLC) is examined to determine the appropriate hydrogen rate of production/consumption for a HGPS [9], however, the simulation results showed that the system does not provide enough input energy to power a typical residential load for a very long time. For a HGPS, comprised of photovoltaic (PV) array, wind turbine, and fuel cells, FLC is employed to achieve maximum power tracking for delivery to a DC bus [10,11].

As the difference in cost of electricity generated by HGPS and non-renewable sources is continuously decreasing due to technological advancements in manufacturing of equipment, it is anticipated that optimal control of HGPS would make the overall system performance even more economical [12]. The optimization of FLC using evolutionary programming has been utilized for different systems, for example, the genetic algorithm (GA) is applied for the simultaneous design of membership functions and rule sets for a FLC of the steam generator water level [13]. This type of controller is smaller and its response is faster than that of a well-tuned proportional–integral–derivative (PID) controller and provides satisfactory performance, although it has a small number of rules. A GA-fuzzy-PID controller is examined for enhancement of energy efficiency of a dynamic energy system [14] and the results show that GA-fuzzy-PID controller, in comparison with PID controller, achieves higher energy efficiency by lowering energy costs. The GA is also used for simultaneously finding optimum design of FLC membership functions and control rules, where the controller

* Corresponding author. Tel.: +98 21 64543323; fax: +98 21 66406469.
E-mail address: ardehali@aut.ac.ir (M.M. Ardehali).

0196-8904/$ - see front matter © 2012 Elsevier Ltd. All rights reserved.
http://dx.doi.org/10.1016/j.enconman.2012.08.012

is used as a maximum-power-point tracker for an autonomous PV panel [15] and the results show improvement in design optimization. The particle swarm optimization (PSO) algorithm is used in a study for tuning a FLC that controls a robot trajectory [16] and it is found to be more accurate with less or no deviation from the trajectory, as compared to a PSO–PID controller. Another application of PSO for designing an optimal FLC for load frequency control of isolated wind-natural gas hybrid power system is reported in [17] and simulation results show that the performance of proposed controller is superior to a PID controller in terms of settling time, overshoot, and robustness under load change. In another study, the PSO algorithm is used for optimizing membership functions of a FLC that controls an autonomous PV panel [18], where the optimized FLC is able to provide maximum energy to the system loads while maintaining a higher average state of charge (SOC) of battery.

As summarized in Table 1, the review of literature shows that studies on optimized FLC for power flow regulation and energy management of HGPS are lacking. The objective of this study is to develop an optimized FLC for operating an autonomous HGPS based on the PSO algorithm. The PSO algorithm is used to optimize the FLC membership functions. Actual data for weekly residential load, wind speed, ambient temperature, and solar irradiation are used for performance simulation and analysis the HGPS. The weekly operation and maintenance (O&M) costs of HGPS is accounted for and, for evaluating reliability of HGPS power production under varying weather conditions, the loss of power supply probability (LPSP) is considered [19].

The remaining parts of this study are organized as follows. In Section 2, the HGPS model is introduced. The analysis section describing the FLC structure, membership functions, and rules as well as the PSO algorithm used for optimizing the FLC membership functions is presented in Section 3. Sections 4 and 5 provide the simulation results and conclusions and recommendations, respectively.

2. HGPS model

As shown in Fig. 1, the HGPS utilizes a wind turbine, a PV array, an electrolyzer, a fuel cell with hydrogen storage tank, and a stack of batteries to meet the load via a DC bus and an inverter [9], where the power flow is regulated by an optimized FLC.

A wind turbine and a PV array are used as indigenous green power production resources. An electrolyzer is used for production and storage of the excess energy in form of hydrogen and a proton exchange membrane fuel cell is used for re-utilization of stored hydrogen to generate electricity. A battery stack is also used to store short-term energy [20]. The buck and boost converters control the electrolyzer and fuel cell power, respectively.

For HGPS simulation in this study, the actual hourly data for load power, wind speed, ambient temperature, and solar irradiation available for the last week of March 2008 in north of Iran are shown in Fig. 2.

2.1. Wind turbine

Based on local wind speed and equipment characteristics, the amount of power produced by wind turbine (kW) is given by [21]

$$P_{wind}(t)=\begin{cases} P_{max,wind}\cdot\frac{V(t)-V_C}{V_R-V_C} & \text{if } V_C\leqslant V(t)\leqslant V_R \\ P_{max,wind} & \text{if } V_R\leqslant V(t)\leqslant V_F \\ 0 & \text{if } V(t)<V_C\cup V(t)>V_F \end{cases} \quad (1)$$

where $V(t)$ is wind speed at time t(m/s), $P_{max,wind}$ is nameplate power rating of wind turbine (kW), V_F, V_R and V_C are the characteristic parameters determined by the wind turbine power curve provided by the manufacturer (m/s), as shown in Fig. 3. The wind turbine starts producing power at a wind speed of 3.5 m/s and reaches rated power at wind speed of 9.5 m/s. At wind speeds higher than 25 m/s, the controller puts the wind turbine on the brake [22].

Table 1
Summary of HGPS studies in the literature.

Reference	Wind	PV	Battery	Hydrogen	Controller	FLC	Optimization
[1]	•	•	•				•
[2]	•	•			•		
[3]	•	•					•
[4]	•	•					•
[5]	•	•	•	•	•		
[6]	•	•		•	•		
[7]	•	•		•	•		
[8]		•	•	•	•		
[9]	•	•	•	•	•		
[10]	•	•		•	•	•	
[11]	•	•		•	•	•	
[12]		•	•		•		
[13]					•	•	•
[14]					•		•
[15]		•			•	•	•
[16]					•	•	•
[17]	•				•	•	•
[18]		•	•		•	•	•
[19]	•	•	•		•		
[20]	•	•	•	•	•		•
[21]	•	•					•
[23]	•	•	•		•		•
[27]					•	•	
[28]	•	•					•
[29]		•	•	•	•		
[30]		•			•		
[31]	•		•	•			•
[32]	•	•	•	•			•
This study	•	•	•	•	•	•	•

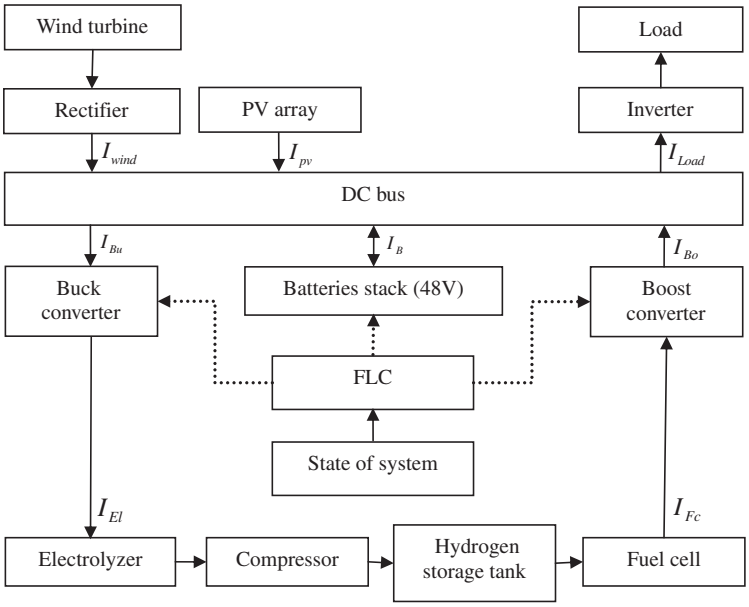

Fig. 1. Schematic diagram of the HGPS used in this study [9].

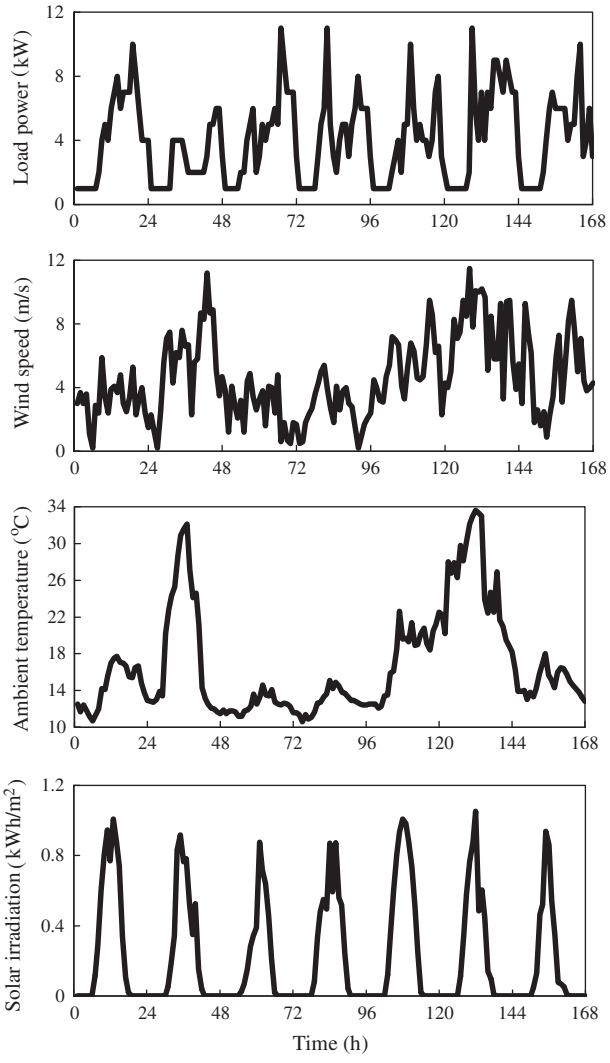

Fig. 2. Hourly data for load power and meteorological conditions for 1 week.

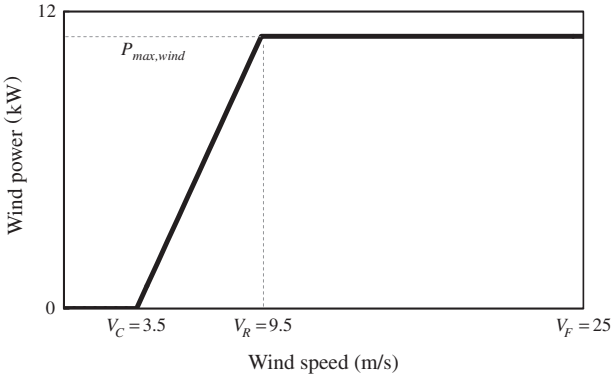

Fig. 3. Wind turbine power production as a function of wind speed [22].

2.2. PV

The power generated (kW) by the PV array with N_S modules in series and N_P modules in parallel, where the effects of temperature is accounted for, is given by [23]

$$P_{pv}(t) = N_P \cdot N_S \cdot \frac{\frac{V_{OC}}{n_{MPP}KT/q} - \ln\left(\frac{V_{OC}}{n_{MPP}KT/q} + 0.72\right)}{1 + \frac{V_{OC}}{n_{MPP}KT/q}} \cdot \left(1 - \frac{R_s}{V_{oc}/I_{sc}}\right) . I_{sco}\left(\frac{G}{G_0}\right)^{\alpha} \cdot \frac{V_{oco}}{1 + \beta \ln\frac{G_0}{G}} \cdot \left(\frac{T_0}{T}\right)^{\gamma} . \eta_{MPPT}\eta_{oth} \quad (2)$$

where n_{MPP} is the ideality factor ($1 < n_{MPP} < 2$), K is the Boltzmann constant (1.38×10^{-23} J/K), T is the PV module temperature (K), q is the magnitude of the electron charge (1.6×10^{-19} °C), R_s is the series resistance (Ω), α is the exponent responsible for all the non-linear effects that the photocurrent depends on, β is a PV module technology specific-related dimensionless coefficient [24], and γ is the exponent considering all the non-linear temperature–voltage effects. Also, V_{oc} and I_{sc} are the open-circuit-voltage (V) and the short-circuit current (A) of the PV module under two different solar

irradiance intensities (G_0, G) and two PV module temperatures (T_0, T), respectively. Further, η_{MPPT} is efficiency of the maximum power point tracking and η_{oth} is the factor representing other losses such as the loss caused by cable resistance and accumulative dust.

2.3. Battery

For the battery stack, the electrical energy storage is positive or negative depending on charging or discharging states. The battery current (A) is determined by [9]

$$I_B(t) = I_{pv}(t) + I_{wind}(t) + I_{Bo}(t) - I_{Bu}(t) - I_{Load}(t) \quad (3)$$

where I_{pv}, I_{wind}, I_{Bo}, I_{Bu} and I_{Load} are currents (A) of PV array, wind turbine, boost converter, buck converter and load, respectively.

The battery voltage (V) is given by

$$U_B(t) = (1 + at)U_{B,0} + R_i I_B(t) + K_i Q_R(t) \quad (4)$$

where a is the self-discharge rate (s^{-1}), $U_{B,0}$ is the open-circuit-voltage at time 0 (V), R_i is the internal resistance (Ω), K_i is the polarization coefficient ($\Omega\,h^{-1}$), and $Q_R(t)$ is the rate of accumulated charge (Ah). The characteristic values for the battery stack parameters are given in Table 2.

Then, the battery energy storage (Ah) is

$$E_B(t) = E_{B,0} + \frac{1}{3600}\int I_B(t)dt \quad (5)$$

where $E_{B,0}$ is the battery initial stored energy (Ah).

The battery SOC (%) is defined by

$$\mathrm{SOC}(t) = 100 \times \frac{E_B(t)}{E_{B,max}} \quad (6)$$

where $E_{B,max}$ is the total capacity of the battery stack (Ah).

Table 2
HGPS components parametric values.

Component	Parameter	Value
PV	α	1.21
	β	0.058
	γ	1.15
	n_{MPP}	1.17
	R_s (Ω)	0.012
	I_{sc} (A)	6.5
	V_{oc} (V)	21
	G_0 (W/m^2)	1000
	T_0 (K)	298
	η_{MPPT}	0.95
	η_{oth}	0.05
Battery	a (Hz)	≈0
	R_i (Ω)	0.076
	$U_{B,0}$ (V)	48
	K_i	≈0
Electrolyzer	$U_{El,0}$ (V)	22.25
	C_{2El} (V)	5.5015
	C_{1El} (V °C^{-1})	−0.1765
	$N_{Cell,El}$	24
	$I_{El,0}$ (A)	0.1341
	$\eta_{I,El}$	0.7
	R_{El} (Ω °C)	−3.3189
	C_{H_2} (Ah l^{-1})	8604
Fuel cell	$U_{Fc,0}$ (V)	33.18
	C_{2Fc} (V)	−1.57
	C_{1Fc} (V °C^{-1})	−0.013
	$N_{Cell,Fc}$	35
	$I_{Fc,0}$ (A)	8.798
	$\eta_{I,Fc}$	0.45
	R_{Fc} (Ω °C)	−2.04
	C_{H_2} (Ah l^{-1})	8604

2.4. Electrolyzer

The excess electrical energy produced by the HGPS is used by the electrolyzer for hydrogen production. The buck converter is a DC voltage reducer used to transfer maximum power from DC bus to the electrolyzer. The electrolyzer voltage (V) is given by [9]

$$U_{El} = U_{El,0} + C_{1El}T_{El}(t) + C_{2El}\ln\left(\frac{I_{El}(t)}{I_{El,0}}\right) + \frac{R_{El}I_{El}(t)}{T_{El}(t)} \quad (7)$$

where $U_{El,0}$ (V), C_{1El} (V °C^{-1}), C_{2El} (V), R_{El} (Ω °C) and $I_{El,0}$ (A) are the characteristic parameters determined experimentally with values given in Table 2 and I_{El} and T_{El} are electrolyzer current (A) and the cell operating temperature (°C), respectively.

The hydrogen production rate $\dot{V}_{El}$ (ls^{-1}) is given by [9]

$$\dot{V}_{El} = N_{Cell,El}\frac{\eta_{I,El}I_{El}(t)}{C_{H_2}} \quad (8)$$

where $N_{Cell,El}$ is the number of cells, $\eta_{I,El}$ is the electrolyzer utilization factor, and C_{H_2} is a conversion coefficient (Ah l^{-1}).

2.5. Fuel cell

For maximizing power transfer between fuel cell and DC bus, the boost converter is utilized. The fuel cell voltage (V) is defined by [9]

$$U_{Fc} = U_{Fc,0} + C_{1Fc}T_{Fc}(t) + C_{2Fc}\ln\left(\frac{I_{Fc}(t)}{I_{Fc,0}}\right) + \frac{R_{Fc}I_{Fc}(t)}{T_{Fc}(t)} \quad (9)$$

where $U_{Fc,0}$ (V), C_{1Fc} (V °C^{-1}), C_{2Fc} (V), R_{Fc} (Ω °C) and $I_{Fc,0}$ (A) are the characteristic parameters, as listed in Table 2, and I_{Fc} and T_{Fc} are fuel cell current (A) and the cell operating temperature (°C), respectively.

The fuel cell hydrogen consumption rate $\dot{V}_{Fc}$ (ls^{-1}) is given by [9]

$$\dot{V}_{Fc} = N_{Cell,Fc}\frac{\eta_{I,Fc}I_{Fc}(t)}{C_{H_2}} \quad (10)$$

where $N_{Cell,Fc}$ and $\eta_{I,Fc}$ are the number of cells and the fuel cell utilization factor, respectively.

2.6. Hydrogen storage

The hydrogen energy storage (kJ) is defined by [9]

$$E_{H_2}(t) = \int_{t=0}^{T}(P_{El} - P_{Fc})dt \quad (11)$$

where P_{El} and P_{Fc} are electrolyzer and fuel cell power (kW), respectively, and T = 168 h in HGPS simulation of this study. The hydrogen storage level (%) is

$$HL = 100 \times \frac{E_{H_2}}{E_{H_2,max}} \quad (12)$$

where $E_{H_2,max}$ is the maximum energy stored in the tank in the form of hydrogen (kJ).

3. Analysis

The optimal performance of HGPS modeled in the previous section is achieved by designing a FLC that benefits from optimum membership functions determined by the PSO algorithm.

3.1. Fuzzy logic controller

A typical fuzzy system takes a state value and passes it through a fuzzification process and, then, it is processed by an inference engine. Finally, it goes through a defuzzification process [25].

As shown in Fig. 1, the FLC is used to regulate energy flow in the HGPS described by Eqs. (1)–(12). The FLC inputs are the net power flow (dp) and the batteries SOC. Note that the net power flow is the difference between the power produced and the power consumed. The FLC output is a power set point (P^*). When P^* is positive, the fuel cell consumes hydrogen as it goes into the operation mode and, when P^* is negative, the electrolyzer begins producing hydrogen.

The membership functions for the FLC inputs and output before optimization, as used by [9], are shown in Fig. 4 and the rules to be evaluated in each hourly time step are shown in Table 3. For membership functions, "N" represents the "Negative" fuzzy set, "Z" represents "Zero", "P" is "Positive", "L" is "Low", "M" is "Medium", and finally "H" is "High". The output is defuzzified using the centroid method [9]. To optimize the membership functions for the inputs and output of the FLC, the PSO algorithm is used [12], as discussed next.

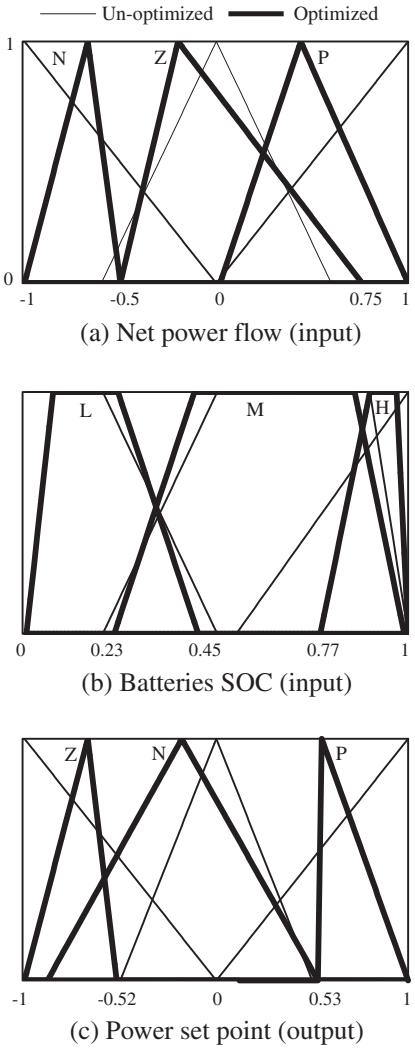

Fig. 4. Inputs and output fuzzy membership functions for un-optimized and optimized FLC ($w = 0.25$).

Table 3
Fuzzy logic rules for HGPS control [9].

dp	SOC	P^*
N	L	P
N	M	P
N	H	N
Z	L	P
Z	M	Z
Z	H	Z
P	L	P
P	M	Z
P	H	N

Table 4
HGPS components cost specifications data [20,21,28,29].

Component	OM_f ($/kW/year)	OM_v ($/kW h)
Wind turbine	10	0
PV array	9.52	0
Fuel cell	0	0.02
Electrolyzer	0	0.0045
Battery	5	0.05

3.2. Particle swarm optimization

The PSO algorithm is a population based optimization method inspired by social behavior of flocks of birds and fish looking for food [26]. Observations show that birds use the information of whole group for finding their direction. Hence, during each flight (iteration), birds as particles update their velocities and positions by the best experience of whole group g_{best} and their own p_{best}. The number of variables in each problem determines the dimension of particles. The quality of solution for each particle is measured by a fitness function evaluated at the particle's current position.

As shown in Fig. 4, three membership functions (two inputs and one output) with three fuzzy sets are considered in this study. The fuzzy sets for the dp and P^* membership functions are represented by triangular functions specified by three values and, for the SOC membership function, the fuzzy set is represented by trapezoidal functions specified by four values. The first and the last values in each membership function are assumed to be fixed. Therefore total of 24 parameters are required to represent the FLC inputs and output membership functions, which implies that each particle in the PSO algorithm has 24 dimensions.

3.3. Performance functions

The two performance functions that are to be minimized by the PSO algorithm include O&M costs and LPSP of the HGPS (Fig. 1). Used by PSO algorithm, an aggregate performance function as a weighted sum of two sub-functions is described by [27]

$$f(x) = w \cdot C_{OM} + (1 - w) \cdot LPSP \tag{13}$$

where $f(x)$, w, C_{OM}, and $LPSP$ are fitness function, weight coefficient, O&M costs function ($), and LPSP function (%), respectively.

The O&M costs is a function of the rated capacity of the equipment and the amount of power generation for each period of operation, respectively [28]

$$C_{OM} = \sum_i P_{max_i} \cdot OM_{f,i} + \sum_i P_{gen_i} \cdot OM_{v,i} \tag{14}$$

where P_{max} (kW) and P_{gen} (kW) denote the rated capacity and generated power of a specific equipment, respectively, OM_f ($/kW) and OM_v ($/kW h) are the fixed and variable O&M costs, and i is technology indicator. $LPSP$ is defined as the probability that an insufficient

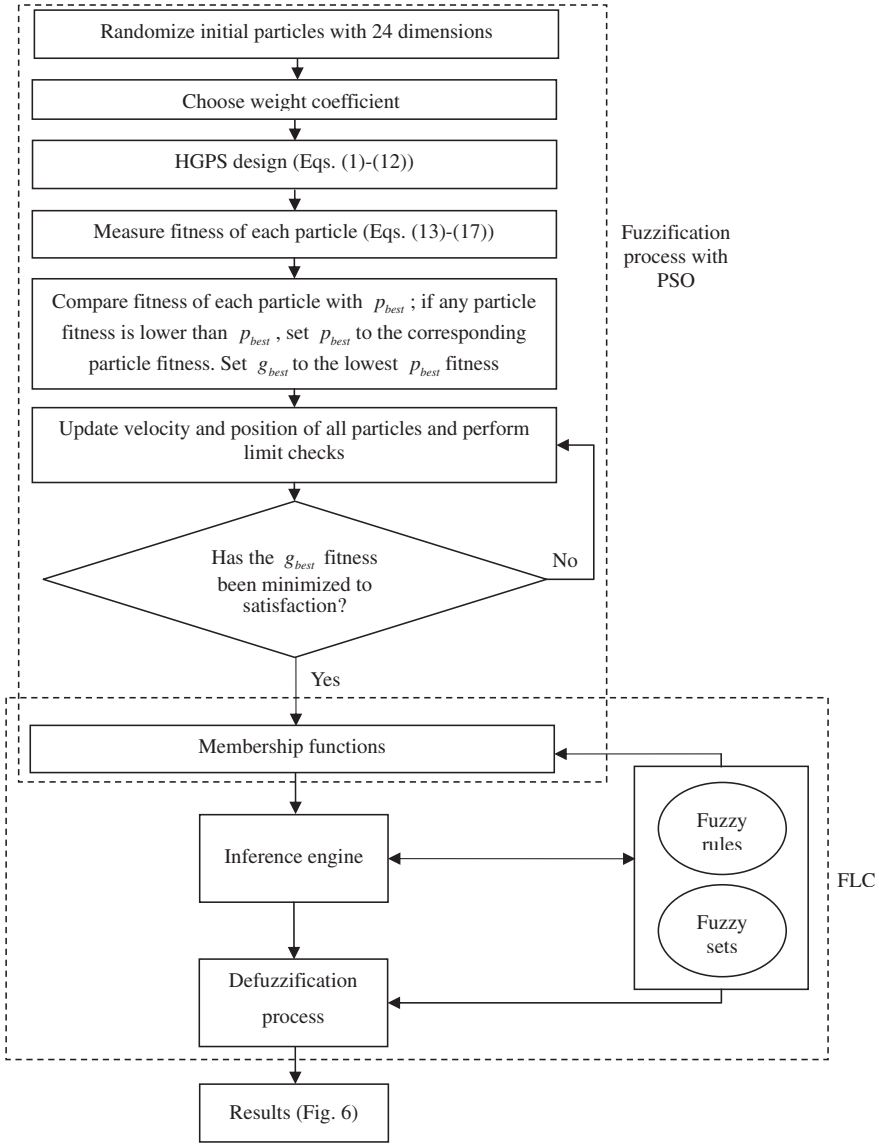

Fig. 5. Flowchart of simulation procedure used in this study.

power supply results, when the HGPS is unable to satisfy the load demand [25]. When *LPSP* = 0, it is implied that the load is satisfied and *LPSP* = 1 means that the load is not satisfied. The LPSP for time 0 to T is described by [23]

$$LPSP = \frac{\sum_{t=0}^{T} Time(P_{available}(t) < P_{needed}(t))}{T} \quad (15)$$

where P_{needed} is the power needed by the load (kW), described by

$$P_{needed}(t) = \frac{P_{load}(t)}{\eta_{inverter}(t)} \quad (16)$$

where P_{load} (t) and $\eta_{inverter}$ are load demand (kW) and inverter efficiency, respectively. $P_{available}$ is the power available from the HGPS (kW), given by

$$P_{available}(t) = P_{pv}(t) + P_{wind}(t) + P_{Fc}(t) + c.U_B(t) \cdot Min\left[I_{B,max} = \frac{0.2C_{bat}}{\Delta t}, \frac{C_{bat} \cdot (\mathrm{SOC}(t) - \mathrm{SOC}_{min})}{\Delta t}\right] \quad (17)$$

where constant c is 0 (battery in charging mode) or 1 (battery in discharging mode), $I_{B,max}$, C_{bat}, Δt and SOC_{min} are maximum battery current (A), available capacity of the battery (Ah), time difference (h) and minimum battery SOC (%), respectively. Table 4 shows the specifications data used for HGPS component cost calculations [20,21,28,29].

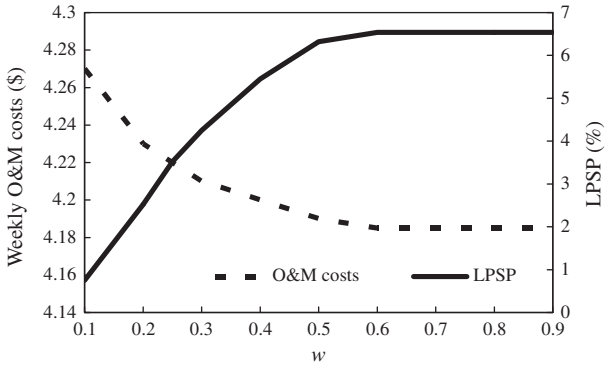

Fig. 6. Variation of O&M costs and LPSP as a function of weight coefficient for optimization.

Table 5
Comparison between results for un-optimized and optimized FLC for 1 week.

Un-optimized FLC					
O&M costs ($)		LPSP (%)		J_{El} (kWh)	J_{Fc} (kWh)
9.84		5.26		37.49	320.51
Optimized FLC					
Weight coefficient	O&M costs ($)	LPSP (%)	Fitness	J_{El} (kWh)	J_{Fc} (kWh)
0.1	4.27	0.75	1.102	4.35	9.41
0.2	4.23	2.52	2.862	10.26	15.24
0.25	4.22	3.52	3.695	40.28	52.36
0.3	4.21	4.25	4.238	100.48	84.98
0.4	4.2	5.45	4.95	65.79	53.82
0.5	4.19	6.32	5.255	36.42	36.46
0.6	4.185	6.54	5.127	36.42	36.46
0.7	4.185	6.54	4.892	36.42	36.46
0.8	4.185	6.54	4.656	36.42	36.46
0.9	4.185	6.54	4.421	36.42	36.46

Table 6
Comparison between costs for HGPS and components [8,20,31,32].

	Wind turbine	PV array	Fuel cell	Electrolyzer	Hydrogen storage tank	Converter	Battery	HGPS cost ($)
Capacity								
Un-optimized	10 kW	6 kW	5 kW	4 kW	130 kW h	5 kW	10 kW h	94,900
Optimized	10 kW	6 kW	2 kW	2 kW	100 kW h	2 kW	5 kW h	77,000
Cost/unit								
	2500 $/kW	6000 $/kW	3000 $/kW	2000 $/kW	30 $/kW	1000 $/kW	200 $/kW h	

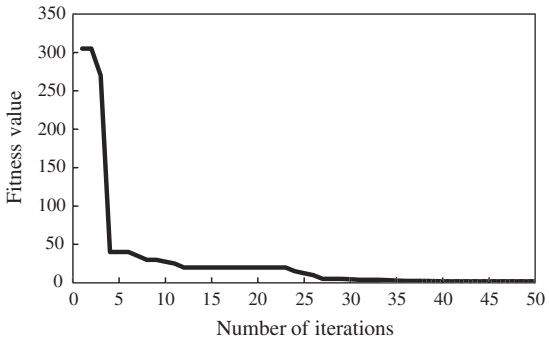

Fig. 7. Convergence of PSO algorithm for optimization ($w = 0.25$).

The electrolyzer energy consumption and the fuel cell energy production are evaluated for 1 week of 24 h operation based on

$$J_{El}(t) = \int_0^t P_{El}dt = \sum_{i=0}^{7\times24} P_{El_i}\Delta t \tag{18}$$

$$J_{Fc}(t) = \int_0^t P_{Fc}dt = \sum_{i=0}^{7\times24} P_{Fc_i}\Delta t \tag{19}$$

4. Simulation results

The flowchart of simulation procedure for HGPS used in this study is shown in Fig. 5. Initial particles with 24 dimensions are randomized from 0 to 1 for SOC fuzzy sets and −1 to 1 for dp and P^* fuzzy sets. For weight coefficient $w = 0.1$–0.9, the fitness function introduced in Eq. (13) is calculated for every particle. The variation of O&M costs and LPSP considering nine possible operational strategies based on varying weights in the aggregate performance function of Eq. (13) are shown in Fig. 6 and the corresponding numeric values are given in Table 5. In Fig. 6, both O&M costs and LPSP remain relatively constant for $w > 0.5$, however, when $0.1 < w < 0.5$, it is observed that there is a continuous increase in LPSP and a continuous decrease in O&M costs. The optimal solution is achieved at $w = 0.25$, where O&M costs = $4.22 and LPSP = 3.52%. It is found that the optimized FLC results in lower O&M costs and LPSP by 57% and 33%, respectively, as compared to those of its un-optimized counterpart. The convergence of PSO algorithm with 50 iterations for optimized FLC, while weight coefficient is 0.25, is shown in Fig. 7. The optimal fuzzy membership functions resulted from the optimization algorithm by PSO for $w = 0.25$ are superimposed over un-optimized membership functions, as shown in Fig. 4. Note that the operation and flow of energy in the HGPS is controlled based on fuzzy rules given in Table 3.

The hourly profile for generated power by wind turbine and PV array as well as un-optimized and optimized storage power and net power delivered by HGPS (= generation + storage) are shown in Fig. 8. For hours 1–3, the PV power is zero and the wind power is less than the load. Considering the un-optimized FLC, the generated power by fuel cells is higher than that required by the load and the excess power is used to charge the battery. It is observed that even when the wind power (1.38 kW) is sufficient to meet the load (1 kW) at hour 4, the fuel cell is in operation with the un-optimized FLC, whereas, the operation of fuel cell is not called for with the optimized FLC and the excess wind power is directed to charge the batteries. When optimized FLC is utilized, for the 24 h operation shown, the required capacities for fuel cells, electrolyzer, and batteries are reduced and HGPS cost is therefore expected to be lowered. It is found that the optimization of FLC membership functions, in general, reduces the fluctuations in operation of the energy storage devises. Further, the power delivered by HGPS is not sufficient to meet load in hours 12 (4 kW), 18 (0.5 kW) and 22 (1 kW), when un-optimized FLC is used, which leads to increase in LPSP. However, for the optimized FLC, the unmet load occurs only in hour 22.

In Fig. 9, the variation of batteries SOC are examined and it is found that it is between 30–65% for un-optimized FLC and between

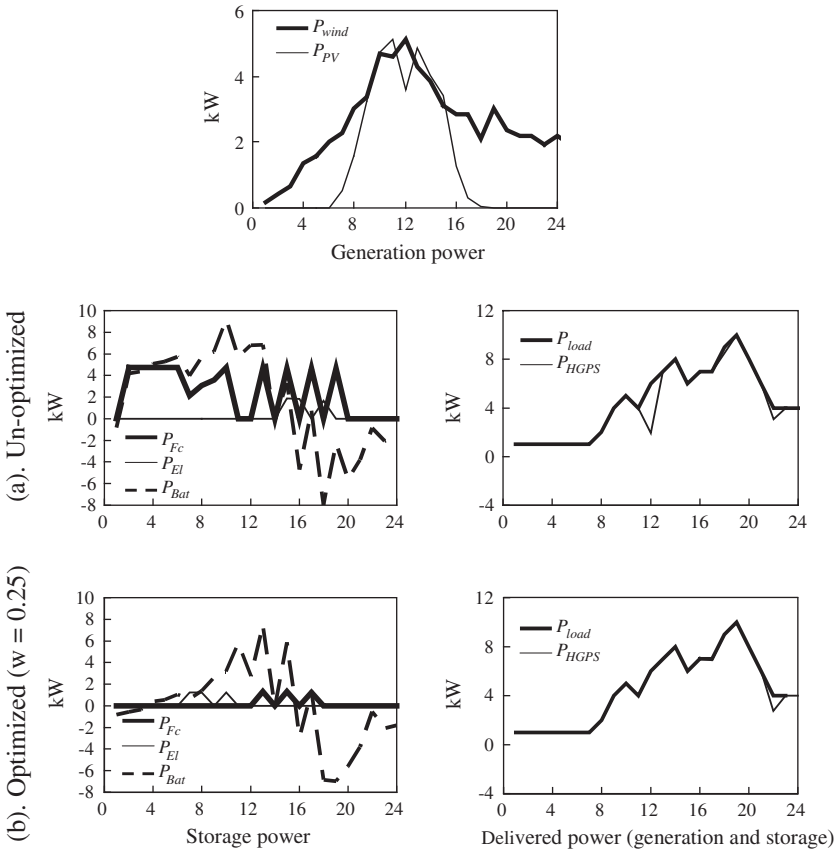

Fig. 8. HGPS power flow using un-optimized and optimized FLC ($w = 0.25$) during 1 day.

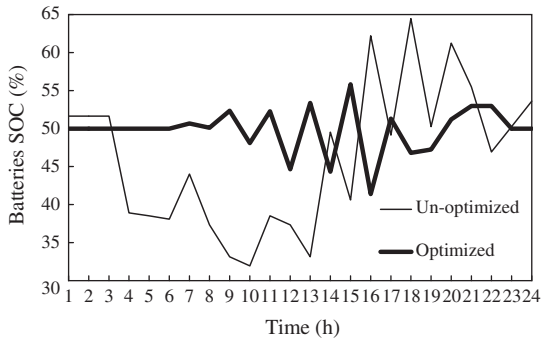

Fig. 9. Batteries SOC with un-optimized and optimized FLC ($w = 0.25$) during 1 day.

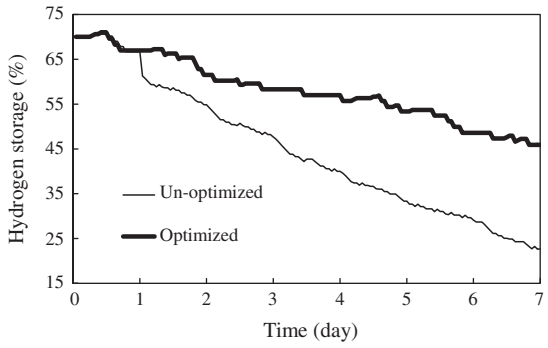

Fig. 10. Hydrogen storage with un-optimized and optimized FLC ($w = 0.25$) during 1 week.

40–56% for optimized FLC. It is determined that the average SOC is 43.8% and 49.98% for un-optimized and optimized FLC, respectively.

The result for hydrogen storage before and after applying optimized FLC is depicted in Fig. 10. While the capacity of the hydrogen storage tank is chosen as 4 m^3 [29], the stored volume for un-optimized and optimized FLC are 1.78 and 2.32 m^3, respectively. The storage tank contains hydrogen by almost 44.5% and 58.03% of its volume for un-optimized and optimized FLC, respectively, which implies lower dependency on hydrogen storage during the operation week of HGPS, when the suggested capacity of 4 m^3 [29] is used.

Base on the simulation results, it is determined that the capacities of the equipment as suggested by [29] are not fully utilized. Because cost reduction opportunities are of high importance, the effects of resizing the equipments capacities are also examined, where the maximum capacities are determined by FLC optimization. The costs of HGPS equipment with different capacities are shown in Table 6, where it is observed that the investment cost for the system utilizing optimized FLC with resized capacities is 18% ($17,900) less than that of HGPS with un-optimized FLC.

5. Conclusions and recommendations

In this study an optimal FLC for a HGPS with hydrogen storage is developed utilizing the PSO algorithm, where the optimization process focuses on FLC membership functions. An aggregate performance function based on O&M costs and LPSP is developed in order to meet the energy demand of an actual weekly residential load while utilizing actual wind, ambient temperature, and solar irradiation data.

In general, the optimization of FLC achieves a superior performance, as compared to that of its un-optimized counterpart. Optimization results in higher average and less variation in SOC of batteries and, as a result, the life of batteries are increased. The reduction in LPSP that is achieved after optimization implies that the load is better met in more hours. In addition, O&M costs are reduced, when FLC is optimized. For further reduction in investment costs for HGPS, the resizing of equipment is accomplished and, as a result, considering the same load profile, smaller equipment would be more suitable and economical.

For future works, the examination of non-autonomous HGPS with optimized FLC and having the ability to sell power to electrical network is recommended.

References

[1] Ardehali MM. Rural energy development in Iran: non-renewable and renewable resources. J Renew Energy 2006;31:655–62.
[2] Little M, Thomson M, Infield D. Electrical integration of renewable energy into stand-alone power supplies incorporating hydrogen storage. Int J Hydrogen Energy 2007;32:1582–8.
[3] Deshmukh MK, Deshmukh SS. Modeling of hybrid renewable energy systems. J Renew Sustain Energy Rev 2008;12:235–49.
[4] Elhadidy MA, Shaahid SM. Parametric study of hybrid (wind + solar + diesel) power generating systems. J Renew Energy 2000;21:129–39.
[5] Muselli M, Notton G, Louche A. Design of hybrid-photovoltaic power generator, with optimization of energy management. J Solar Energy 1999;695:143–57.
[6] Onar OC, Uzunoglu M, Alam MS. Modeling, control and simulation of an autonomous wind turbine/photovoltaic/fuel cell/ultra-capacitor hybrid power system. J Power Sources 2008;185:1273–83.
[7] Zhou T, Lu D, Fakham H, Francois B. Power flow control in different time scales for a wind/hydrogen/super-capacitors based active hybrid power system. In: Proc EPE-PEMC, Poznan, Poland; 2008. p. 2205–10.
[8] Vosen SR, Keller JO. Hybrid energy storage systems for stand-alone electric power systems: optimization of system performance and cost through control strategies. Int J Hydrogen Energy 1999;24:1139–56.
[9] Bilodeau A, Agbossou K. Control analysis of renewable energy system with hydrogen storage for residential applications. J Power Sources 2006;162:757–64.
[10] El-Shatter TF, Eskander MN, El-Hagry MT. Energy flow and management of a hybrid wind/PV/fuel cell generation system. J Energy Convers Manage 2006;47:1264–80.
[11] Ahmed NA, Miyatake M, Al-Othman AK. Power fluctuations suppression of stand-alone hybrid generation combining solar photovoltaic/wind turbine and fuel cell systems. J Energy Convers Manage 2008;49:2711–9.
[12] Welch RL, Venayagamoorthy GK. Energy dispatch fuzzy controller for a grid-independent photovoltaic system. J Energy Convers Manage 2010;51:928–37.
[13] Na MG. Design of a genetic fuzzy controller for the nuclear steam generator water level control. J IEEE Trans Nucl Sci 1998;45:2261–71.
[14] Jahedi G, Ardehali MM. Genetic algorithm-based fuzzy-PID control methodologies for enhancement of energy efficiency of a dynamic energy system. J Energy Convers Manage 2011;52:725–32.
[15] Messai A, Mellit A, Guessoum A, Kalogirou SA. Maximum power point tracking using a GA optimized fuzzy logic controller and its FPGA implementation. J Solar Energy 2011;85:265–77.
[16] Bingul Z, Karahan O. A fuzzy logic controller tuned with PSO for 2 DOF robot trajectory control. J Expert Syst Appl 2011;38:1017–31.
[17] Chokpanyasuwan C, Pothiya S, Anantasate S, Bhasaputra P. Optimal fuzzy logic controller design using particle swarm optimization for wind-natural gas power system. In: 6th International conference on ECTI-CON. 01 (6–9 May 2009), Thailand 164–167.
[18] Welch RL, Venayagamoorthy GK. Comparison of two optimal control strategies for a grid independent photovoltaic system. In: IEEE industry application society 41st annual meeting. 3 Tampa, FL; 2006. p. 1120–27.
[19] Yang HX, Lu L, Burnett J. Weather data and probability analysis of hybrid photovoltaic–wind power generation systems in Hong Kong. J Renew Energy 2003;28:1813–24.
[20] Milo A, Gaztanaga H, Etxeberria Otadui I, Bacha S, Rodriguez P. Optimal economic exploitation of hydrogen based grid-friendly zero energy buildings. J Renew Energy 2011;36:197–205.
[21] Ren H, Gao W. A MILP model for integrated plan and evaluation of distributed energy systems. J Appl Energy 2010;87:1001–14.
[22] Installation Manual Gaia-Wind 11 kW Turbine. August 2008, GW-UK-18-0808 User Manual. <http://www.dcpower-systems.com/documents/Gaia-WindUser-Manual.pdf>. [accessed 09.07.11, 10.08.12].
[23] Hongxing Y, Wei Z, Lin L, Zhaohong F. Optimal sizing method for stand-alone hybrid solar–wind system with LPSP technology by using genetic algorithm. J Solar Energy 2008;82:354–67.
[24] Van Dyk EE et al. Long-term monitoring of photovoltaic devices. Renew Energy 2002;22:183–97.
[25] Engelbercht AP. Computational intelligence: an introduction. 2nd ed. John Wiley & Sons; 2007.
[26] Kennedy J, Eberhart R. Particle swarm optimization. In: Proceedings of the IEEE international conference on neural networks. 4, Perth, WA, Australia; 27 November–1 December 1995.
[27] Ardehali MM, Saboori M, Teshnelab M. Numerical simulation and analysis of fuzzy PID and PSD control methodologies as dynamic energy efficiency measures. J Energy Convers Manage 2004;45:1981–92.
[28] Ren H, Zhou W, Nakagami K, Gao W, Wu Q. Multi-objective optimization for the operation of distributed energy systems considering economic and environmental aspects. J Appl Energy 2010;87:3642–51.
[29] Pedrazzi S, Zini G, Tartarini P. Complete modeling and software implementation of a virtual solar hydrogen hybrid system. J Energy Convers Manage 2010;51:122–9.
[30] Zhou W, Yang H, Fang Z. A novel model for photovoltaic array performance prediction. J Appl Energy 2007;84:1187–98.
[31] Khan MJ, Iqbal MT. Pre-feasibility study of stand-alone hybrid energy systems for applications in newfoundland. J Renew Energy 2005;30:835–54.
[32] Agbossou K, Chahine R, Hamelin J, Laurencelle F, Anouar A, St-Arnaud JM, et al. Renewable energy systems based on hydrogen for remote applications. J Power Sources 2001;96:168–72.